Chinese Chemical Letters 34 (2023) 107144

Contents lists available at ScienceDirect

Chinese Chemical Letters

journal homepage: www.elsevier.com/locate/cclet

Electrochemically exfoliated Ni-doped MoS_2 nanosheets for highly efficient hydrogen evolution and Zn-H_2O battery

Hao Wei[a,b,1], Jincheng Si[a,b,1], Libin Zeng[b,c], Siliu Lyu[b], Zhiguo Zhang[a], Yange Suo[a,*], Yang Hou[b,d,**]

[a] School of Mechanical and Energy Engineering, Zhejiang University of Science and Technology, Hangzhou 310027, China
[b] Key Laboratory of Biomass Chemical Engineering of Ministry of Education, College of Chemical and Biological Engineering, Zhejiang University, Hangzhou 310027, China
[c] Institute of Zhejiang University - Quzhou, Quzhou 324000, China
[d] School of Metallurgy and Chemical Engineering, Jiangxi University of Science and Technology, Ganzhou 341000, China

ARTICLE INFO

Article history:
Received 3 December 2021
Revised 5 January 2022
Accepted 13 January 2022
Available online 19 January 2022

Keyword:
Electrochemical exfoliation
Ni doping
MoS_2
Hydrogen evolution reaction
Zn-H_2O battery

ABSTRACT

Thanks to tunable physical and chemical properties, two-dimensional (2D) materials have received intensive interest, endowing their excellent electrocatalytic performances for applications in energy conversion. However, their catalytic activities are largely determined by poor adsorption energy and limited active edge sites. Herein, a one-step electrochemical exfoliation strategy was developed to fabricate 2D Ni-doped MoS_2 nanosheets (Ni-EX-MoS_2) with a lateral size of ~500 nm and thickness of ~3.5 nm. Profiting from high electrical conductivity and abundant exposing active sites, Ni-EX-MoS_2 catalyst displayed an admirable performance for electrochemical hydrogen evolution reaction (HER) with a low overpotential of 145 mV at 10 mA/cm^2 as well as a small Tafel slope of 89 mV/dec in alkaline media, which are superior to those of the most reported MoS_2-based electrocatalysts. The formed Ni species with tuning electronic structure played a crucial role as primary active center of Ni-EX-MoS_2, as well as the forming stable 1T/2H phase MoS_2 interface demonstrated a synergistic effect on electrocatalytic HER performance. Further, Ni-EX-MoS_2 was employed as a cathode electrode for alkaline Zn-H_2O battery, which displayed a high power density of 3.3 mW/cm^2 with excellent stability. This work will provide a simple and effective guideline for design of electrochemically exfoliated transition metal-doped MoS_2 nanosheets to inspire their practical applications in energy catalytic and storage.

© 2022 Published by Elsevier B.V. on behalf of Chinese Chemical Society and Institute of Materia Medica, Chinese Academy of Medical Sciences.

With ever-increasing global energy needs and the intensification of environmental pollution, new renewable energy conversion technologies have been inevitably attracting much attention [1–5]. Electrochemical water splitting to generate green H_2 is a sustainable and environmentally friendly strategy. As one of two half-cell reactions of water splitting, hydrogen evolution reaction (HER) is a key step and has been extensively studied in the last decades [6–10]. Noble metal catalysts, especially Pt-based materials, are still the most efficient electrocatalysts for HER [2,11]. However, the high cost and scarcity of noble Pt catalyst greatly hinder their large-scale commercial applications. Thereupon, the development of low-cost and efficient catalysts for electrochemical water splitting is of great importance [12,13].

Recently, transition metal dichalcogenides (TMDs) materials have been regarded as promising alternatives for Pt-based catalysts due to their abundant exposed edge sites and excellent electron mobility along the nanosheets [13,14]. Among them, molybdenum sulfide (MoS_2) is one of the most promising TMDs candidates for HER because of its favorable electronic structure, good corrosion resistance, and high stability [14,15]. Nevertheless, local exposed active sites and inherent poor conductivity largely suppress the HER performance of bulk-phase MoS_2 [15–18]. Therefore, several strategies have been proposed to improve their catalytic performances. For up-to-down strategy, exfoliating bulk MoS_2 into two-dimensional (2D) layer-like MoS_2 nanosheets is an encouraging approach, which can obtain monolayer/few-layer MoS_2 with large surface area as well as rich exposed active sites [18–20]. Unfortunately, due to the multistep synthesis reactions, the conventional exfoliation methods, such as mechanical exfoliation [21], liquid

* Corresponding author.
** Corresponding author at: Key Laboratory of Biomass Chemical Engineering of Ministry of Education, College of Chemical and Biological Engineering, Zhejiang University, Hangzhou 310027, China.
E-mail addresses: suoyange@zust.edu.cn (Y. Suo), yhou@zju.edu.cn (Y. Hou).
[1] The authors contributed equally to this work.

https://doi.org/10.1016/j.cclet.2022.01.037
1001-8417/© 2022 Published by Elsevier B.V. on behalf of Chinese Chemical Society and Institute of Materia Medica, Chinese Academy of Medical Sciences.

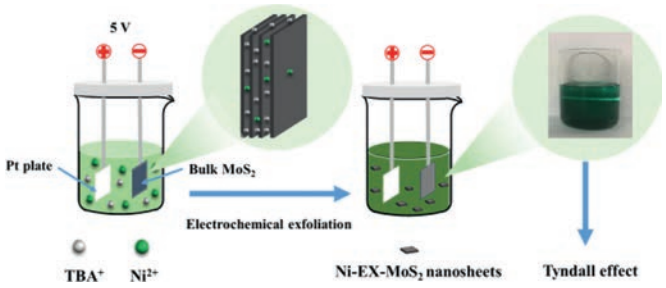

Fig. 1. Schematic diagram of the electrochemical exfoliation and synthetic procedure.

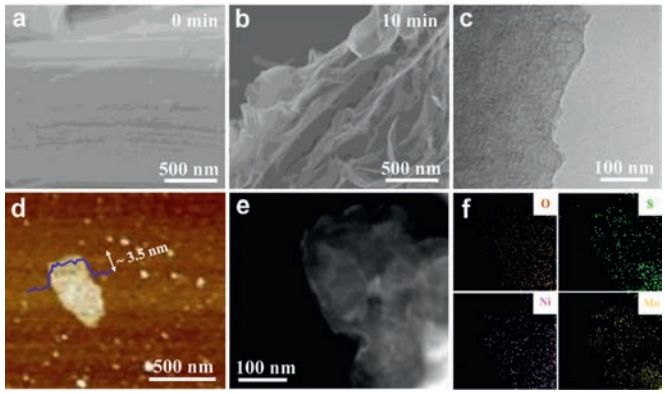

Fig. 2. SEM images of (a) bulk MoS_2 and (b) Ni-EX-MoS_2. (c) TEM image of Ni-EX-MoS_2. (d) AFM image of Ni-EX-MoS_2. (e) HAADF-STEM image of Ni-EX-MoS_2. (f) EDX elemental mapping images of O, S, Ni and Mo in the corresponding region.

sonication exfoliation [22], and lithium-ion intercalation [23] are usually hard to control the number of layers and thickness of 2D nanosheets. Compared with these reported methods, electrochemical exfoliation route has attracted great interest owing to its simple procedure, high efficiency as well as good controllability, and it has been successfully applied to the exfoliation of most 2D materials, such as phosphorene, graphene, and WS_2 [24]. Besides, transition metals doped TMDs materials can efficiently modulate hydrogen adsorption/desorption energy to enhance whole electrocatalytic activity [24–26]. Especially, the doping of Ni atoms could optimize the electronic structure of MoS_2, regulate the electron density of Mo atom [26], which would reduce the free energy of hydrogen adsorption and boost catalytic performance. Therefore, it is desirable to develop an effective method for rapid exfoliation production of TMDs and *in situ* doping of transition metal to improve their HER performance. In this work, a usual 2D Ni-doped MoS_2 (Ni-EX-MoS_2) nanosheets was prepared through a one-step electrochemical exfoliation treatment of bulk MoS_2 in a mixture electrolyte of *N,N*-dimethylformamide (DMF) and tetrabutylammonium bromide (TBAB). The obtained Ni-EX-MoS_2 catalyst with a thickness of ~3.5 nm and a lateral dimension of ~500 nm, exhibited an excellent HER activity, featured by a low overpotential of 145 mV at 10 mA/cm^2 and a small Tafel slope of 89 mV/dec in 1.0 mol/L KOH, which was ascribed to the formation of 2D 1T/2H-MoS_2 heterojunction and doping of Ni species during the exfoliation process. Intriguingly, the Ni-EX-MoS_2 could also be employed as a cathode electrode for alkaline Zn-H_2O battery with a power density up to 3.3 mW/cm^2 and good stability of ~6.0 h.

A schematic diagram of the synthetic route for Ni-EX-MoS_2 was presented in Fig. 1. Bulk MoS_2 was firstly synthesized by a solid phase reaction in a sealed quartz tube by annealing a mixture of Mo and S powders. Then, as-prepared bulk MoS_2 was used as cathode and underwent an electrochemical exfoliation at 5.0 V for 10 min with TBA^+ (6 mg/mL) in $NiCl_2$ $6H_2O$ (5 mg/mL)/DMF electrolyte to obtain Ni-EX-MoS_2 nanosheets. The cathodic bulk MoS_2 was polarized by the specific electric field and a negative charge was generated on the surface. The TBA^+ and Ni^{2+} ions in the electrolyte could migrate to the bulk MoS_2, and then the TBA^+ ions intercalates into the interlayer of bulk MoS_2, which causes the expansion of MoS_2 interlayers. Meanwhile, the Ni^{2+} ions was intercalated into MoS_2 interlayer, which was further trapped by the negatively charged exfoliated MoS_2. A final product of Ni-EX-MoS_2 nanosheets was subsequently collected by ultrasonic shaking, centrifugation, and freeze-drying steps. The operation details refer to the section of experimental synthesis and the main products are synthesized under these conditions, except for special markings.

As shown in Fig. S1 (Supporting information), X-ray diffraction (XRD) patterns of bulk MoS_2 and Ni-EX-MoS_2 showed the main peak located at 14.2°, which was attributed to the (002) crystal plane of MoS_2 crystal [27]. After the electrochemical exfoliation, the peak intensity on the (002) plane of Ni-EX-MoS_2 was much weaker than that of bulk MoS_2, which can be attributed to the thinner layered structure formed in the Ni-EX-MoS_2 [20,28]. No signal peaks of Ni-related species were detected. The morphologies of bulk MoS_2 and Ni-EX-MoS_2 were explored by field emission scanning electron microscopy (FESEM) images. As shown in Figs. 2a and b, few-layer Ni-EX-MoS_2 nanosheets was successfully synthesized by the electrochemical exfoliation from original multilayered stacked bulk MoS_2. Transmission electron microscopy (TEM) (Fig. 2c) and atomic force microscopy (AFM) images (Fig. 2d) showed that the Ni-EX-MoS_2 nanosheets processed a lateral size of ~500 nm and a thickness of ~3.5 nm, corresponding to five layers stacked together (single-layer thickness of 0.62 nm for MoS_2) [29,30]. Atomic-resolution high-angle annular dark-field scanning TEM (HAADF-STEM) image in Fig. 2e revealed the flat surface of Ni-EX-MoS_2 without obvious particles formed. Moreover, energy dispersive X-ray spectroscopy (EDX) mapping images displayed the homogenous distribution of Ni, Mo and S elements throughout the whole Ni-EX-MoS_2 nanosheet structure (Fig. 2f), respectively. The content of Ni species in the Ni-EX-MoS_2 catalyst was determined to be 4.8% by inductively coupled with plasma atomic emission spectroscopy (ICP-AES) analysis (Table S1 in Supporting information).

Considering that the magnitude of voltage plays a key role in the electrochemical exfoliation process, the exfoliation quality and particle size of MoS_2 nanosheets were furtherly explored at other applied voltages (3.0 and 10 V). At a voltage of 3.0 V, the MoS_2 surface produced little negative electrical attraction to TBA^+ ions, which made it difficult to intercalate into the interlayer of bulk MoS_2, thus leading to poor exfoliation. As a result, the large-sized multilayer MoS_2 sheets was obtained (Fig. S2a in Supporting information). In contrast, when the applied voltage was increased to 10 V, it resulted in a higher intercalation rate and the faster disruption of the van der Waals forces between bulk MoS_2 layers, thus leading to the smaller crystal sizes for few-layer MoS_2 nanosheets (Fig. S2b in Supporting information). Due to the moderate intercalation rate and amount of TBA^+ ions into the MoS_2 interlayer, the Ni-EX-MoS_2 with high quality was obtained at the voltage of 5.0 V.

Fig. 3a showed the enlarged HRTEM image of Ni-EX-MoS_2 nanosheets. Unambiguously, it is observed the coexistence of 1T and 2H phases MoS_2 in the plane (marked with red and yellow circles). The interplanar spacings of 0.27 and 0.27 nm in the yellow region can be attributed to the (010) and (100) crystal faces of 2H phase MoS_2, respectively [19]. While the interplanar spacing of 0.27 nm in the red region could be assigned to the (101) crystal face of 1T phase MoS_2 [31], which indicates that the original 2H-phase MoS_2 was partially transformed into 1T-phase MoS_2 after electrochemical exfoliation [29,32]. Obviously, it can be iden-

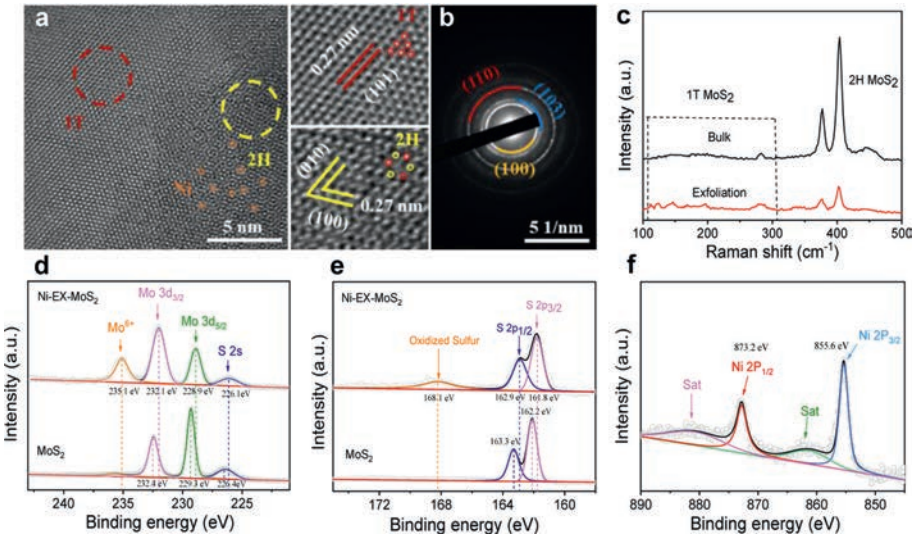

Fig. 3. (a) HRTEM images Ni-EX-MoS_2 nanosheets. Inset: red and yellow dots in the atomic arrangement of 1T and 2H phases represent for Mo and S atoms. (b) Corresponding SAED pattern. (c) Raman spectra of Ni-EX-MoS_2 and bulk MoS_2. High-resolution XPS spectra of (d) Mo 3d, (e) S 2p and (f) Ni 2p, respectively.

tified the doped Ni atoms (marked with orange circles) and continuous lattice streaks of the 1T-2H phase within the section. As displayed in Fig. 3b, the diffraction rings in the selected area electron diffraction (SAED) for Ni-EX-MoS_2 can be indexed to the (100), (110) and (103) facets of MoS_2. Raman spectra was used to characterize the bulk MoS_2 and Ni-EX-MoS_2 catalysts (Fig. 3c), where the characteristic peaks located at 379.3 and 405.9 cm^{-1} are attributed to the in-plane (E^1_{2g}) and out-of-plane (A_{1g}) modes of 2H phase MoS_2 [33,34]. In addition, several additional peaks appeared at 147.6 and 226.1 cm^{-1}, corresponding to J_1 and J_2 vibrational modes of S-Mo-S bonds in 1T-phase MoS_2 [19,35]. These results demonstrated that the partial phase transformation occurred from the 2H-phase MoS_2 to 1T-phase MoS_2 after the electrochemical exfoliation.

To further explore the electronic structures of Ni-EX-MoS_2, the measurements of X-ray photoelectron spectroscopy (XPS) were conducted. The full-survey XPS spectrum presented Ni, Mo, and S elements in the Ni-EX-MoS_2 (Fig. S3 in Supporting information). In high-resolution Mo 3d XPS spectra (Fig. 3d), bulk MoS_2 showed two peaks located at 232.4 and 229.3 eV, which corresponds to the characteristic Mo $3d_{5/2}$ and Mo $3d_{3/2}$ peaks of 2H phase MoS_2, respectively [27,36]. For the Ni-EX-MoS_2, it showed three peaks centered at 235.1, 232.1, and 228.9 eV corresponding to the characteristic peaks of Mo^{6+}, Mo $3d_{5/2,}$ and Mo $3d_{3/2}$, respectively [36,37]. The decrease in the binding energy was probably due to the shift of Fermi energy level, as additional electrons populated the d orbitals caused by the partial phase transition, as verified by the coexistence of 1T and 2H phases MoS_2 heterojunction [38,39]. In Fig. 3e, the high-resolution S 2p XPS spectra of the Ni-EX-MoS_2 displayed two peaks located at 162.9 and 161.8 eV, which are assigned to the characteristic peaks of S $2p_{1/2}$ and S $2p_{3/2}$, respectively. Compared with the S $2p_{1/2}$ (163.3 eV) and S $2p_{3/2}$ (162.2 eV) peaks of bulk MoS_2 with 2H phase, the corresponding peaks of Ni-EX-MoS_2 decreased a 0.4 eV in binding energy, further demonstrating the formation of 1T phase MoS_2 in the Ni-EX-MoS_2 [38,39]. A new characteristic peak in the sulfur oxidation state was found in Fig. 3e, which might be due to the oxidation of the Ni-EX-MoS_2 when exposed to air during the XPS test [20]. The peaks located at 873.2 and 855.6 eV in Fig. 3f can be assigned to Ni $2p_{1/2}$ and Ni $2p_{3/2}$, respectively, in consistent well with the previous report [40]. Based on HRTEM, Raman, and XPS results, one can conclude that the rapid electrochemical exfoliation enables synchronous exfoliation of bulk MoS_2 and incorporation of Ni species into Ni-EX-MoS_2 nanosheets.

The electrocatalytic HER activities of the Ni-EX-MoS_2 were evaluated using a three-electrode cell in 1.0 mol/L KOH. All polarization curves were recorded with iR compensation. For comparison, the reference samples including bulk MoS_2 and EX-MoS_2 were also tested. As shown in Fig. 4a, commercial Pt/C exhibited the highest HER activity. In addition, the Ni-EX-MoS_2 displayed the excellent HER performance with an overpotential as low as 145 mV at 10 mA/cm^2, much lower than those of MoS_2 (>600 mV at 10 mA/cm^2) and EX-MoS_2 (425 mV at 10 mA/cm^2), respectively. Furthermore, the Tafel slope of Ni-EX-MoS_2 was measured to be 89 mV/dec, which was lower than those of EX-MoS_2 (96 mV/dec) and MoS_2 (121 mV/dec) (Fig. 4b), demonstrating excellent HER kinetic property [41].

To further clarify the intrinsic activity of Ni-EX-MoS_2, the electrochemically active surface areas (ECSA) of the catalysts were estimated by the electrochemical double-layer capacitance (C_{dl}, Figs. S4a–c in Supporting information). The Ni-EX-MoS_2 showed the largest C_{dl} value of 3.78 mF/cm^2 as compared to the EX-MoS_2 (2.21 mF/cm^2) and bulk MoS_2 (1.11 mF/cm^2), suggesting more exposed active sites in the Ni-EX-MoS_2 (Fig. S4d in Supporting information). In addition, the tests of electrochemical impedance spectroscopy (EIS) showed that the charge-transfer resistance (R_{ct}) value of Ni-EX-MoS_2 was 101 Ω, which was smaller than that of EX-MoS_2 (196 Ω) and bulk MoS_2 (1022 Ω), respectively, indicating that the Ni-EX-MoS_2 possessed a faster electron transfer capability (Fig. 4c and Table S2 in Supporting information). Notably, the as-prepared Ni-EX-MoS_2 exhibited an outstanding HER catalytic activity with low Tafel slope and small overpotential, which was superior to most of previously reported MoS_2-based HER electrocatalysts under alkaline conditions (Fig. 4d and Table S3 in Supporting information).

Fig. S5a (Supporting information) showed a multicurrent step curve for the Ni-EX-MoS_2 with the current densities being cumulative from 5.0 mA/cm^2 to 25 mA/cm^2. Likewise, the corresponding multipotential step curve of Ni-EX-MoS_2 was also displayed in Fig. S5b in Supporting information. All other steps showed the same trends, which presented the outstanding mass transport property and superior mechanical robustness of Ni-EX-MoS_2 [42]. Further durability tests showed that Ni-EX-MoS_2 had excellent stability in alkaline media, with negligible potential drop after 8 h of contin-

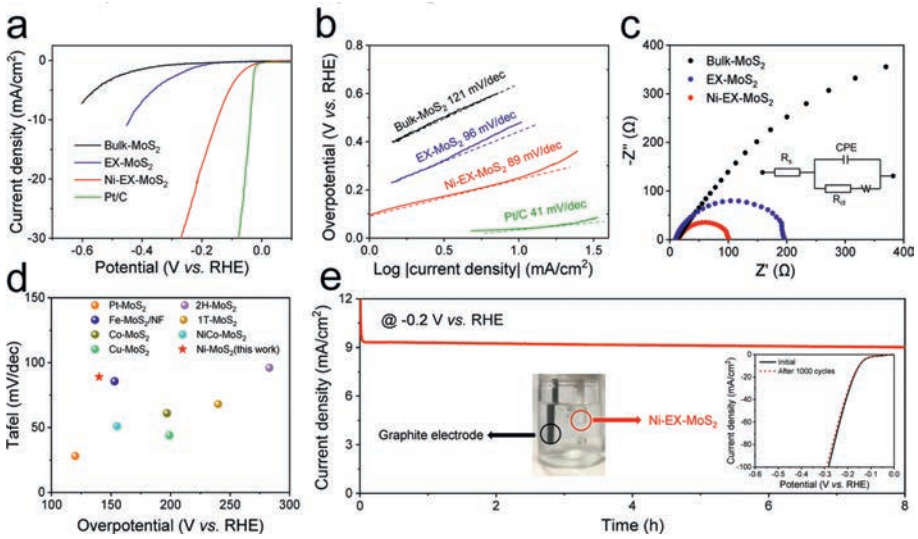

Fig. 4. (a) Polarization curves of bulk MoS_2, EX-MoS_2, Ni-EX-MoS_2, and Pt/C after iR-correction and (b) Tafel plots of bulk MoS_2, EX-MoS_2, Ni-EX-MoS_2 and Pt/C in 1 mol/L KOH solution. (c) Nyquist plots of bulk MoS_2, EX-MoS_2, Ni-EX-MoS_2. Inset: An equivalent circuit for fitting impedance data. (d) Comparison of overpotentials at 10 mA/cm^2 and Tafel slopes with recently reported MoS_2-based electrocatalysts. (e) Chronopotentiometry curve of Ni-EX-MoS_2 without iR-correction. Inset: photograph for electrochemical stability at 10 mA/cm^2. Inset: polarization curves of Ni-EX-MoS_2 for the first and 1000th CV cycles.

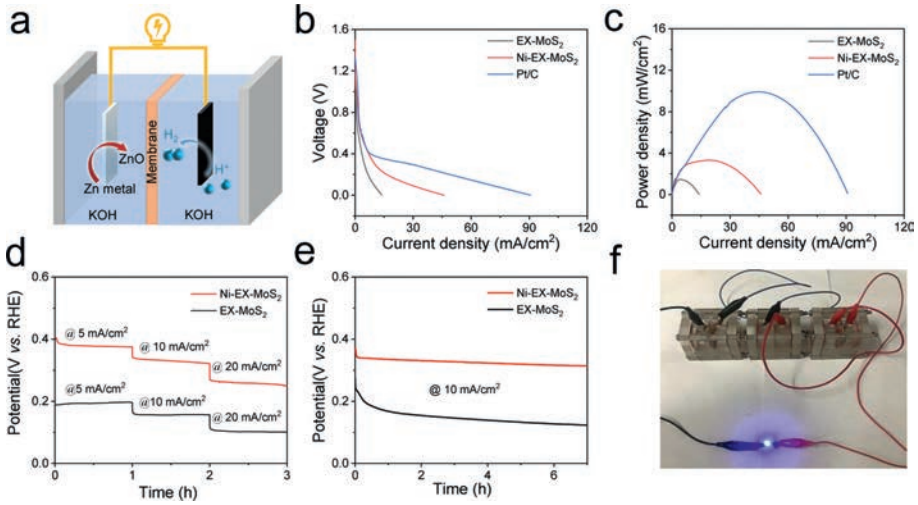

Fig. 5. (a) Schematic illustration of Zn-H_2O battery. (b) Discharge polarization curves of EX-MoS_2, Ni-EX-MoS_2 and Pt/C. (c) Corresponding power density curves. (d) Chronopotentiometric responses of EX-MoS_2, Ni-EX-MoS_2, and Pt/C-based Zn-H_2O battery at current densities ranging from 5 mA/cm^2 to 20 mA/cm^2 during discharging process. (e) Galvanostatic discharge curves at 10 mA/cm^2. (f) Actual photograph of a blue light-emitting diode lit by three series-connected Ni-EX-MoS_2-based Zn-H_2O batteries.

uous HER process (Fig. 4e). This conclusion was further supported by inset of Fig. 4e, no obvious change in the polarization curves of Ni-EX-MoS_2 before and after 1000 cycles was observed.

To clarify the HER mechanism of Ni-EX-MoS_2, a series of experiments and analyses were carried out. Firstly, we used the thiocyanate ions (SCN^-), which is considered as a toxic effect on Ni species, to reveal the real active site of Ni-EX-MoS_2. It is evident that after the addition of SCN^- ions, the current density of Ni-EX-MoS_2 suddenly decreased and the potential dropped from 0.18 V to 0.35 V (Fig. S6 in Supporting information), demonstrating the effective blocking of active Ni sites. Besides, the high-resolution XPS spectra of Ni 2p, Mo 3d and S 2p on the Ni-EX-MoS_2 before and after HER tests were compared (Fig. S7 in Supporting information). In the high-resolution XPS spectrum of Ni 2p, the binding energy of Ni 2p was significantly increased after HER catalysis, indicating a higher valence state of Ni species in the Ni-EX-MoS_2 [43,44]. Further, the Ni-EX-MoS_2 showed a positive shift of 0.5 eV of Ni 2p peak during the HER process, which can be attributed to the electrons transferred from the Ni center to the adjacent H_2 molecules [45,46]. These results revealed that the Ni species in the Ni-EX-MoS_2 was acted as the main active center for HER. The post-TEM and post-HRTEM characterizations demonstrated that the lamellar structures and lattice stripes were almost unchanged after the HER reaction (Figs. S8a–c in Supporting information). The presence of uniformly distributed Ni species (Fig. S8d in Supporting information) and the coexistence of 1T and 2H phases of MoS_2 (Fig. S8b) on the base of Ni-EX-MoS_2 demonstrated its strong durability.

Moreover, in order to verify the general applicability of this electrochemical exfoliation strategy, the different kinds of TMDs materials induced by doping of other metals (Fe, Co, Ni and Mn) were also explored, and this synthetic strategy of the electrochemical exfoliation with simultaneous metal doping was experimentally demonstrated to enhance HER activity (Fig. S9 in Supporting information). Especially, the Co-EX-$MoSe_2$ and Co-EX-WSe_2 catalysts displayed a greater improvement in HER activity than those of the corresponding bulk phases.

To further realize the efficient application of simultaneous H_2 and electricity production, the Ni-EX-MoS_2 based Zn-H_2O fuel battery in 1.0 mol/L KOH was constructed (Fig. 5a). When the battery started to discharge, an oxidation reaction occurred at anode Zn plate, while the HER happened at the cathode [47–50]. The commercial Pt/C-based Zn-H_2O battery displayed the best electrochemical performance. Fig. 5b showed the discharge polarization curves of the Zn-H_2O battery with different cathode materials. The Ni-EX-MoS_2 exhibited a higher current density than that of the control EX-MoS_2 during the discharge process. Moreover, the Ni-EX-MoS_2-based Zn-H_2O battery reached a high power density of 3.3 mW/cm^2 (Fig. 5c), exceeding the EX-MoS_2-based battery (1.5 mW/cm^2). In Fig. 5d, no significant loss of voltage at different current densities of 5, 10, 15 and 20 mA/cm^2 was observed for the Ni-EX-MoS_2 based Zn-H_2O battery, indicating the excellent stability of Ni-EX-MoS_2-based Zn-H_2O battery. During the discharge process, the specific capacities of the Zn-H_2O battery at 5 mA/cm^2 was calculated to be 826 mAh/g (Fig. S10 in Supporting information). In addition, the Ni-EX-MoS_2-based Zn-H_2O battery exceeded the chronopotentiometry curve for 6 h at 10 mA/cm^2 with insignificant voltage change, which indicates outstanding durability of this Zn-H_2O battery (Fig. 5e). Significantly, Fig. 5f illustrated that three Zn-H_2O batteries connected in series light up a blue light-emitting diode, which indicates that the proposed Zn-H_2O battery shows a great perspective in terms of energy supply.

In summary, a novel 2D Ni-EX-MoS_2 nanosheets catalyst, with a lateral size of ~500 nm and thickness of ~3.5 nm, was synthesized *via* a one-step electrochemical exfoliation strategy. During the synthesis processes, the simultaneous electrochemical exfoliation and the doping of Ni species were beneficial to the formation of a stable 1T/2H phase-MoS_2 heterojunction, which endowed the Ni-EX-MoS_2 with the higher conductivity and more active sites, thus led to the excellent HER activity in base. In addition, the Ni-EX-MoS_2 acted as a cathode of the Zn-H_2O battery displayed a high power density as well as good stability during the HER process. This work might provide new avenues for the development of other transition metal-doped 2D TMDs for various meaningful applications in electrochemistry, including N_2 reduction reactions, CO_2 reduction, and O_2 reduction reactions.

Declaration of competing interest

The authors declare that they have no known competing financial interests or personal relationships that could have appeared to influence the work reported in this paper.

Acknowledgments

This work is financially supported by the National Natural Science Foundation of China (Nos. 21805244, 51776188). We also greatly acknowledg the financial support from National Natural Science Foundation of China (Nos. 21922811, 21878270, 21961160742), the Zhejiang Provincial Natural Science Foundation of China (No. LR19B060002), the Startup Foundation for Hundred-Talent Program of Zhejiang University, Jiangxi Province "Double Thousand Plan" Project (No. 205201000020).

Supplementary materials

Supplementary material associated with this article can be found, in the online version, at doi:10.1016/j.cclet.2022.01.037.

References

[1] Y.N. Xia, C.T. Campbell, B.R. Cuenya, et al., Chem. Rev. 121 (2021) 563–566.
[2] Y. Hou, M. Qiu, M.G. Kim, et al., Nat. Commun. 10 (2019) 1392.
[3] C.X. Zhao, J.N. Liu, J. Wang, et al., Chem. Soc. Rev. 50 (2021) 7745.
[4] C.X. Zhao, J.N. Liu, J. Wang, et al., Adv. Mater. 33 (2021) 2008606.
[5] X.M. Liu, X.Y. Cui, K. Dastafkan, et al., J. Energy Chem. 53 (2021) 290.
[6] C.J. Lei, H.Q. Chen, J.H. Cao, et al., Adv. Energy Mater. 8 (2018) 1801912.
[7] I.T. McCrum, M.T.M. Koper, Nat. Energy 5 (2020) 891–899.
[8] L.K. Zheng, L.N. Hu, Y.C. Hu, et al., Catal. Sci. Technol. 11 (2021) 3706.
[9] H. Yang, S. Gao, C.N. Zhang, et al., Sci. China Chem. 64 (2021) 101–108.
[10] Q. Li, Y.C. Wang, J. Zeng, et al., Chin. Chem. Lett. 32 (2021) 3355–3358.
[11] Q.R. Shi, C.Z. Zhu, D. Du, et al., Chem. Soc. Rev. 48 (2019) 3181–3192.
[12] Y. Hou, M. Qiu, T. Zhang, et al., Adv. Mater. 29 (2017) 170158.
[13] Q. Fu, X.J. Han, X.J. Wang, et al., Adv. Mater. 33 (2021) 1907818.
[14] J.F. Zhang, T.Y. Zhu, Y. Wang, et al., Mater. Today 36 (2020) 83–90.
[15] J.J. Wei, G. Wang, Y.J. Zhang, et al., Chin. Chem. Lett. 32 (2021) 1191–1196.
[16] P. Prabhu, V. Jose, J.M. Lee, Matter 2 (2020) 526–553.
[17] Y.K. Rao, H.D. Wang, Y.J. Zeng, et al., Adv. Sci. 8 (2021) 2002284.
[18] X.L. Pan, M.Y. Yan, C.L. Sun, et al., Adv. Funct. Mater. 31 (2021) 2007840.
[19] H. Niu, Zou Z.G, Q. Wang, et al., Chem. Eng. J. 399 (2020) 125675.
[20] J.C. Si, Q. Zheng, H.L. Chen, et al., ACS Appl. Mater. Interfaces 11 (2019) 13205–13213.
[21] X. Wang, J.J. He, B.Q. Zhou, et al., Angew. Chem. Int. Ed. 57 (2018) 8668–8673.
[22] Q. Xu, Y.B. Zhu, T.T. Xie, et al., ChemCatChem 13 (2020) 592–602.
[23] Y.T. Luo, X. Li, X.K. Cai, et al., ACS Nano 12 (2018) 4565–4573.
[24] D.N. Liu, J.H. Wang, J. Lu, et al., Small Methods 3 (2019) 1900083.
[25] X.P. Li, C. Huang, W.K. Han, et al., Chin. Chem. Lett. 32 (2021) 2597–2616.
[26] J.J. Wu, J. Peng, Y. Zhou, et al., J. Am. Chem. Soc. 141 (2019) 592–598.
[27] X. Wang, Y.W. Zhang, H.N. Si, et al., J. Am. Chem. Soc. 142 (2020) 4298–4308.
[28] J.C. Si, H.L. Chen, C.J. Lei, et al., Nanoscale 11 (2019) 16200–16207.
[29] X. Hai, W. Zhou, S.Y. Wang, et al., Nano Energy 39 (2017) 409–417.
[30] K. Wu, X. Cao, M.Y. Li, et al., Small 16 (2020) 2004178.
[31] B. Pattengale, Y.C. Huang, X.X. Yan, et al., Nat. Commun. 11 (2020) 4114.
[32] D.Z. Wang, X.Y. Zhang, S.Y. Bao, et al., J. Mater. Chem. A 5 (2017) 2681–2688.
[33] X.L. Zheng, Z.H. Guo, G.Y. Zhang, et al., J. Mater. Chem. A 7 (2019) 19922–19928.
[34] J. Zhang, T. Wang, P. Liu, et al., Energy. Environ. Sci. 9 (2016) 2789–2793.
[35] K. Sun, Y.Q. Liu, Y. Pan, et al., Nano. Res. 11 (2018) 4368–4379.
[36] S.A. Shah, L. Xu, R.N. Sayyar, et al., Chem. Eng. J. 428 (2022) 132126.
[37] X.Y. Meng, C. Ma, L.Z. Jiang, et al., Angew. Chem. Int. Ed. 59 (2020) 10502–10507.
[38] W.W. Yang, S.Q. Zhang, Q. Chen, et al., Adv. Mater. 32 (2020) 2001167.
[39] H.Q. Jin, Y. Yu, Q.K. Shen, et al., J. Mater. Chem. A 9 (2021) 13996–14003.
[40] X.Y. Yu, Y. Feng, Y. Jeon, et al., Adv. Mater. 28 (2016) 9006–9011.
[41] L. Wang, Z.J. Li, K.X. Wang, et al., Nano Energy 74 (2020) 104850.
[42] F.P. Cheng, L. Wang, H.Q. Wang, et al., Nano Energy 71 (2020) 104621.
[43] H. Wang, Z.J. Li, Y. Li, et al., Nano Energy 81 (2021) 105613.
[44] C.J. Lei, Y. Wang, Y. Hou, et al., Energy. Environ. Sci. 12 (2019) 149–156.
[45] H. Wang, J.C. Si, T.Y. Zhang, et al., Appl. Catal. B 270 (2020) 118892.
[46] Z.Y. Yu, Y. Duan, M.R. Gao, et al., Chem. Sci. 8 (2017) 968–973.
[47] H. Li, M.T. Zhang, L.C. Yi, et al., Appl. Catal. B 280 (2021) 119412.
[48] P.W. Cai, Y. Li, G.X. Wang, et al., Angew. Chem. 130 (2018) 3974–3979.
[49] Y.C. Ding, P.W. Cai, Z.H. Wen, Chem. Soc. Rev. 50 (2021) 1495–1511.
[50] M.T. Zhang, H. Li, P.W. Cai, et al., Adv. Funct. Mater. 31 (2021) 2103248.